IEEE Access
Multidisciplinary | Rapid Review | Open Access Journal

Received July 24, 2021, accepted August 11, 2021, date of publication August 20, 2021, date of current version August 27, 2021.

Digital Object Identifier 10.1109/ACCESS.2021.3106343

Temperature-Insensitive Label-Free Sensors for Human IgG Based on S-Tapered Optical Fiber Sensors

HAOWEI LIU[1], YUNXU SUN[1], (Senior Member, IEEE), JUN GUO[2], WEI LIU[1], LE LIU[2], YAN MENG[1], AND XIN YU[1]

[1]State Key Laboratory on Tunable Laser Technology, School of Electronic and Information Engineering, Harbin Institute of Technology at Shenzhen, Shenzhen, Guangdong 518055, China
[2]Tsinghua Shenzhen International Graduate School, Shenzhen, Guangdong 518055, China

Corresponding author: Yunxu Sun (sunyunxu@hit.edu.cn)

This work was supported by Shenzhen Municipal Science and Technology Plan Project, China, under Grant JCYJ20160427183803458 and Grant JCYJ20190806142611.

ABSTRACT We demonstrate a temperature-insensitive and high-sensitive label-free biosensor for low-concentration Human IgG detection based on S-tapered optical fiber (STF). The sensor is sensitive to local refractive index changes and has high robustness against temperature noise without a temperature control system. The temperature sensitivity of the sensor is −0.02nm/°C in the range of 25°C-45°C. Within 15 minutes at room temperature, the average drift of the center wavelength is 0.04 nm. The calibration experiments demonstrate that STFs for liquid achieved a sensing precision of 0.04 nm and a sensitivity of 538.62 nm/RIU. The STFs are applied for the concentration measurement of multiple diluted ex vivo IgG biomolecule solutions. The results showed that STFs were reliable for low-concentration IgG detection and its lower limit of measurement was demonstrated as 28 ng/ml. With the advantages of temperature-insensitive, compact size, low cost, high precision, real-time detection, fast response, good specificity, this STF sensors are promising for the antigen detection applications.

INDEX TERMS Human IgG, high precision, S-tapered fiber biosensor, temperature-insensitive.

I. INTRODUCTION

The concentration of human immunoglobulin G (IgG) is generally considered as one important physiological indicator of the immune response. Therefore, the detection and analysis of human IgG were significant for clinical diagnosing and drug development [1]–[3]. However, IgG is sparse in blood vessels and the development of high-sensitivity biosensors has been a growing interest during the past decades [4]. The traditional detection methods of IgG antigen, such as enzyme-linked immunosorbent assay (ELISA) [5], radioimmunoassay (RIA) [6], and high-performance liquid chromatography (HPLC) [7], suffer from high cost, multi-step processing, and long detection time. Recently, various optical biosensors have been developed for quantifying molecular information using the electrochemical method [8], [9], surface plasmon resonance (SPR) [10], [11], and fiber optics [12], [13]. Among them, optical fiber sensors based on intermodal interference have become one of the major optical sensing techniques, which can sense the changes of external refractive index, temperature, humidity, strain, displacement, pH value, and other parameters in time by converting these changes into optical signals such as interference peak wavelength [14]–[19]. So far, intermodal interference has been realized in single-mode fiber, multimode fiber, and photonic crystal, based on which multiple types of fiber sensor have been developed, such as tilted fiber Bragg grating sensor [20], fiber sensor based on partial core fusion [21], fiber sensor based on mode field mismatch [22], etc. The tapered sensors have the advantages of simple structure, small volume, and strong evanescent field, which can achieve a high detection sensitivity.

The S-tapered fiber (STF) sensor is one type of tapered fiber, which bend at the taper transition where the high-order modes are excited. STFs performs as micro Mach-Zehnder interferometers (MZI) on fibers, which demonstrate high

The associate editor coordinating the review of this manuscript and approving it for publication was Sukhdev Roy.

sensitivity and robustness, firstly proposed by Rui yang *et al.* in 2011 [23]. Afterward, the STF sensors attract substantial interest and are applied to detect refractive index (RI) and strain [24]–[27]. STF sensors may provide a new approach for high-sensitivity and lower-cost sensing of human IgG.

In this paper, we demonstrate an STF biosensor with high sensitivity and temperature insensitive for low-concentration detection, which is verified by the detection of Human IgG. The detection of human IgG is crucial in the prevention of cancer, chronic infection, and influenza virus. Therefore, it is significant to measure the concentration of Human IgG accurately and sensitively.

II. CHARACTERIES OF STF SENSOR

A. PRINCIPLE

The STF sensor is a fiber Mach-Zehnder interferometer (MZI), comprising two abrupt bending sections and one straight waist section as shown in Fig. 1. The field of cladding mode extends out of the fiber in the waist section and interacts with the adjacent environment as a sensing arm while the core mode is confined inside the fiber core as the reference arm. STF's structural parameters, such as the axial offset length, the diameter of the waist section, and bending section, will all affect the transmission characteristics of the STF. However, these parameters are mainly related to the stretched length and axial offset of the optical fiber. Therefore, we will study the influence of different stretch and axial offset length on the transmission characteristics of STF.

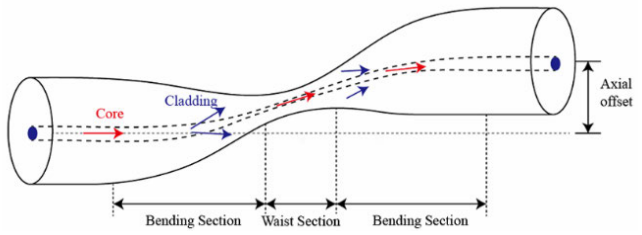

FIGURE 1. Schematic diagram of STF sensor.

According to the two-mode interference, the intensity of the output light can be expressed as:

$$I = I_1 + I_2 + 2\sqrt{I_1 I_2}\cos(\Delta\phi) \tag{1}$$

where I_1 and I_2 are the intensities of the fundamental core mode and the high order cladding mode, respectively. $\Delta\phi$ is the phase difference between the two modes, which is defined as:

$$\Delta\phi = 2\pi \left(n_{eff}^{co} - n_{eff}^{cl}\right) L / \lambda \tag{2}$$

where L is the effective interference length. λ is the light wavelength. n_{eff}^{co} and n_{eff}^{cl} are the effective refractive indices of the fiber core and fiber cladding respectively. n_{eff}^{co} remains constant while n_{eff}^{cl} changes according to the local environment refractive index. The peak wavelength of the transmission spectrum can be derived as:

$$\lambda_m = 2\pi \Delta n_{eff} L / (2m + 1) \tag{3}$$

where m is the interference order.

On the other hand, temperature changes will cause both Δn_{eff} and L to change, resulting in a change in phase difference. The corresponding wavelength shift can be derived as:

$$\Delta\lambda \approx [(\alpha + \xi)\Delta T]\lambda \tag{4}$$

where α is the thermal expansion coefficient of the silica fiber and ξ is the difference of the thermo-optic coefficient of the two modes [28]. ξ being a function of the fiber profile can be either positive or negative on the fiber diameter. In addition, changes in temperature will also cause changes in the refractive index of the liquid, which will also change the interference wavelength. At a particular diameter, the negative can compensate for the thermal expansion effect. In consequence, the wavelength shift may be small.

B. PERFORMANCE OF STF SENSOR

STF is fabricated from single-mode fiber using a tapering machine by an electric arc (Shandong Coupler technology CO., LTD AEBT-8000LE-H). We are using standard single-mode communication fiber (Corning SMF-28) with core and cladding diameters of 9 μm and 126 μm, respectively. As shown in Fig.2, the whole experimental platform consists of five parts: electric arc heating head, electric control generator, optical fiber clamping platform, three-dimensional micro displacement operation platform and computer software control system. Firstly, the optical fiber is placed straight in the central groove of the fiber clamping platform and keep in a tight state through the three-dimensional micro displacement operation platform. Then, the fiber is fused by electric arc heating. Finally, the STF is obtained by stretching the optical fiber in the opposite direction through the electronic control displacement platform and applying transverse displacement. The stretching length and axial offset of STF can be controlled by computer. The two ends of the optical fiber sample are respectively connected with a broadband light source and a spectrometer to monitor the transmission spectrum.

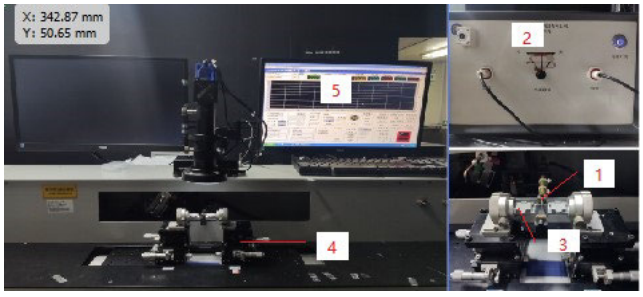

FIGURE 2. Optical fiber taper machine. 1–electric arc heating head; 2–electric control generator; 3–optical fiber clamping platform; 4–three-dimensional micro displacement operation platform; 5–computer software control system.

Broadband light sources (BBS, Fiberlake, ASE) with wavelengths ranging from 1250nm to 1650nm were used as an input light source. The output spectrum of the STF sensor was measured by an optical spectrum analyzer (OSA, Yokogawa aq6370c, Japan), with a resolution of 0.02 nm.

We explore the relationship between the structural parameters of STF and its transmission spectra. Fig.3 gives STF sensors with different waist lengths of 400,500,600,700 and 800 μm and the same axial offsets as 160 μm. As shown in Fig.3 f), the S-tapper fiber with 500, 600, 700, and 800 μm corresponds to 5, 4, 3, and 2 interference dip respectively, and the number of resonant peaks and dips decreases in turn.

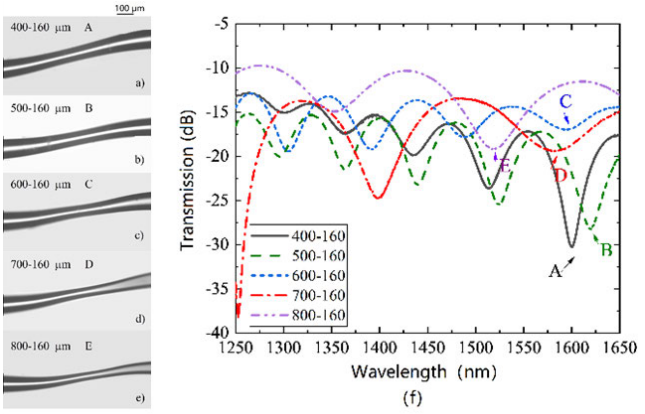

FIGURE 3. STFs with different stretch lengths and the spectrum. a) - e) optical microscope images of STF with different axial offsets when the axial offsets is fixed at 160 μm. f) The transmission spectrum of SFT corresponding to a) - e).

Following, STF sensors with the axial offsets of 80, 120, 160, 200, and 240 μm, and with the same waist length of 700 μm. The optical microscope image and transmission spectrum of these STF sensors are shown in Fig.4. It can be seen from the figure that the extinction ratio of each STF first increases and then decreases. The reason for this change is that a certain value of axial offset can break the structural symmetry and promote the excitation of higher-order modes. However, when the axial offset is too large, most of the energy is dissipated in the form of bending loss, and the energy of the fundamental mode and higher-order mode participating in the interference process decreases.

The transverse offset of S-tapered fiber will affect the contrast of the transmission spectrum. The too large or too small lateral offset will lead to too small excitation energy in S-tapered fiber and decrease the contrast of the transmission spectrum. When the stretching length is 700 μm and the axial offset is 160 μm, the contrast of the S-tapered fiber transmission spectrum is the largest.

The S-tapered fiber sensor with a label prepared before was selected. Because the S-tapered fiber sensor with tensile length and axial offset was set as 700 μm and 160 μm has good mechanical strength and proper interference contrast, we select the sensor to process our experiment. The waist

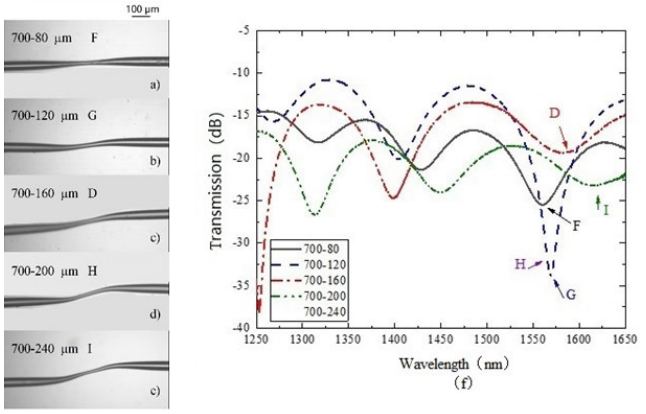

FIGURE 4. STFs with different axial offsets and the spectrum. a) - e) optical microscope images of STF with different taper waist diameters when the stretching length is fixed at 700 μm. f) The transmission spectrum of STF corresponding to a) - e).

diameter and axial offset were measured to be 75.3 μm and 160.1 μm respectively.

C. EXPERIMENT METHOD

As shown in Fig 5 (a), we have fabricated an STF sensor with a taper length (L) of 1507 μm, a waist diameter (d) of 53 μm, and an axial offset (Loff) of 163 μm. Fig. 5 (b) illustrates the detection system consisting of a circulation section and a sensing section. In the circulation part, a flow cell is used to circulate the sensing liquid and ensure the stability of the sensor. The flow cell is constructed using Polydimethylsiloxane (PDMS) which includes two liquid inlet and outlet channels, and the two liquid channels are arranged axially in the middle of the PDMS. A directional cavity is constructed in the middle of the liquid inlet and outlet channels to make the liquid fully contact the sensor. Keep the flow rate of the liquid constant during the circulation of the sensing liquid to maintain the stability of the measurement.

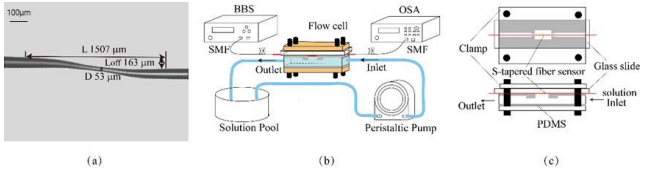

FIGURE 5. STF sensor, experimental system and microchannel. (a) The microscopic images of the STF sensor. (b) The schematic diagram of the detection system. (c) The structure of flow cell.

STF sensor is fixed on the slide that is clamped on the flow cell upside down, as shown in Fig. 5 (c). Therefore, the STF sensor passes through the flow cell and is completely immersed in the solution. With the help of a peristaltic pump (pre fluid, mp300, China), the test solution is extracted from the solution pool, injected into the flow cell through the inlet pipe, and then pushed out of the flow cell from the outlet pipe. In the sensing part, the STF sensor is embedded into the flow cell.

III. RESULT AND DISCUSSION

A. TEMPERATURE INSENSITIVITY

Temperature drift is a key disturbance for the performance of sensors. So, we study the temperature response of STF sensor. Firstly, STF sensor is placed in a constant temperature water bath, and the temperature is changed from 25 °C to 85 °C at 10 degree intervals. The transmission spectrum of STF has little change, shown in Fig.6 (a). We selected the temperature ranges of 25°C-45°C and 45°C-85°C for linear fitting and obtained the temperature sensitivity. When the taper diameter is in the range of 40-90 μm, the STF sensor is in a negative temperature coefficient sensing area [28]. At each temperature, we measure data 10 times to calculate the uncertainty of measurement. The maximum of the standard deviations is 0.08nm.

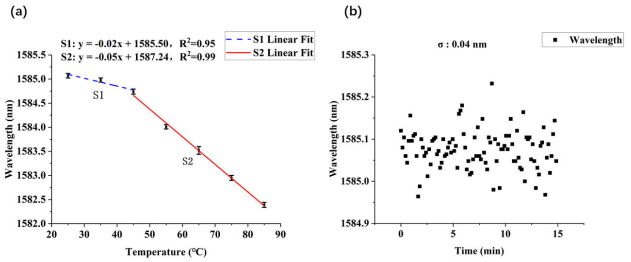

FIGURE 6. (a) The shift of Dip with temperature (b) Variation of trough wavelength of d S-tapered fiber in 15 minutes without temperature control system.

Further, a long-time test of the STF sensor is demonstrated without any temperature control, the transmission spectrum of STF is collected in a deionized water liquid environment in 15 minutes at room temperature. The spectral wavelength drift is shown in Fig 6 (b). The σ was 0.04 nm. Therefore, our STF sensor is suitable for temperature-independent refractive index sensing near room temperature and has good temperature stability. Therefore, the following experiments were carried out at room temperature without temperature control.

B. CALIBRATION OF STF SENSOR FOR REFRACTIVE INDEX SENSING

The refractive index sensing ability of STF is calibrated out by measuring different concentrations of sodium chloride solution. We have prepared deionized water and sodium chloride solutions with concentrations of 0mg/ml, 20mg/ml, 40mg/ml, 60mg/ml, and 80mg/ml. The refractive indices of the solutions measured by the Abbe refractive index are 1.3317, 1.3345, 1.3378, 1.3415, and 1.3436 respectively. Every solution of a certain concentration circulates in the flow channel pool for 3 minutes. The corresponding spectral data of the spectrometer are recorded, and then the channel cell and pipeline are cleaned with deionized water for the next test. The transmission spectrum of the STF sensor in sodium chloride solution was obtained, as shown in Fig.7.

In order to describe the specific performance of the sensor, two dips with high interference contrast of STF sensor are

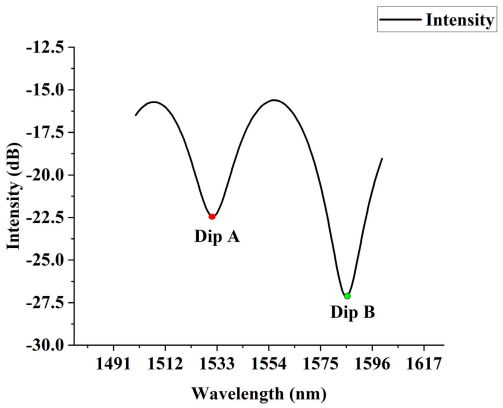

FIGURE 7. The spectrums of the STF sensor in sodium chloride solution.

selected as Dip A, Dip B, and the two dips are tracked and recorded. The spectral data corresponding to the two interference dips marked by an S-tapered fiber sensor are shown in Fig.8(a) and Fig.8(b). It can be seen from the figure that with the increase of solution concentration, the external refractive index will also increase, and the spectrum will shift to a long wavelength.

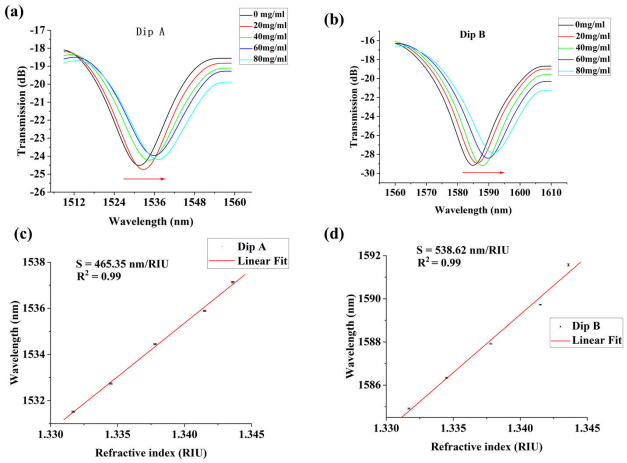

FIGURE 8. (a) The experimental data and linear fit results of Dip A; (b) The experimental data and linear fit results of Dip B; (c) The wavelength shift of Dip A with the variation of the RI; (d) The wavelength shift of dip B with the variation of the RI.

The central wavelengths corresponding to the two interference troughs are determined and the corresponding refractive index sensitivity is calculated. The results are shown in Fig.8(c) and Fig.8(d). The corresponding sensitivities of Dip A and B are 465.35 nm/RIU and 538.62 nm/RIU, respectively. The fitting linearity was 0.99 and 0.99, respectively. At each concentration, 10 real-time spectral data were acquired continuously. The results show that the uncertainties of Dip A and Dip B are both 0.02nm. It can be seen that for multiple interference dips of the same S-tapered fiber, the refractive index sensitivity at the long wavelength is higher than that at the short wavelength and has good stability

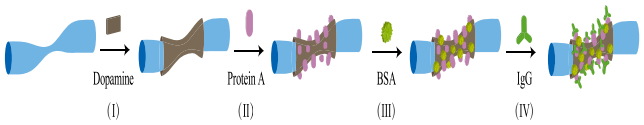

FIGURE 9. The main procedures of the surface functionalization and Protein A-IgG binding reaction.

for the measurement of the concentration of each sodium chloride solution.

C. BIOSENSING OF STF SENSOR

At first, the deionized water is injected into the flow cell by the peristaltic pump and circulated for 10 minutes to create a clear and stable baseline. Then, the 2 mg/ml dopamine solution is mixed with 10 mM Tris-HCl buffer (pH 8.5). The mixture is circulated in the flow cell for 10 minutes to create a multifunctional adhere platform based on the oxidative polymerization of the dopamine aqueous solution, as step (I) shown in Fig. 9. After 5 minutes of circulation of the deionized water and the PBS buffer, the 100 μg/ml Protein A solution in PBS buffer is circulated for 30 minutes for enough contact with the sensor. The Protein A molecules are immobilized on the surface to build up a specific recognition layer, as step (II). The 500 μg/ml BSA solution in the PBS buffer washes the flow cell for 10 minutes to block the uncombined polydopamine sites after circulating 5 minutes PBS buffer, as step (III). The STF sensors are functionalized for biosensing.

Finally, different concentrations of IgG solutions in 100 mM PBS buffer (pH 7.5) are circulated 50 min for a complete binding reaction, as step (IV), followed by another 5 minutes circulation of PBS buffer and 10 minutes flow of the deionized water..

Fig.10 shows the shift of interference spectrum during the whole process of fiber surface functionalization and antigen-antibody binding. Equation (3) indicates that for cladding modules, The n_{eff} decreases with the decrease of the surrounding refractive index, resulting in λ_m will move towards the short wavelength, also known as blue shift.

Due to the self-assembly of dopamine on the fiber surface, STF Sensor show a wavelength shift of about 1.678 nm. the adsorption of protein A fixed on the dopamine nanolayer contributes another wavelength shift of 0.176 nm.

IgG antigen can react with protein A on the surface of optical fiber, resulting in the interference wavelength moving further 0.766 nm to the shorter wavelength region within 25 minutes. With the further increase of time, the wavelength does not shift significantly, which indicates that the binding of antigen and antibody has reached saturation as a complete process of antibody-antigen binding. In Fig. 10, The two inset graphics indicate the change of the interference wavelength of the sensor in PBS buffer before and after the immune response. Before immune reaction, the interference wavelength of fiber in PBS buffer is 1477.023 nm, and the corresponding variance is 0.03 nm. After the immune reaction, the interference wavelength of the

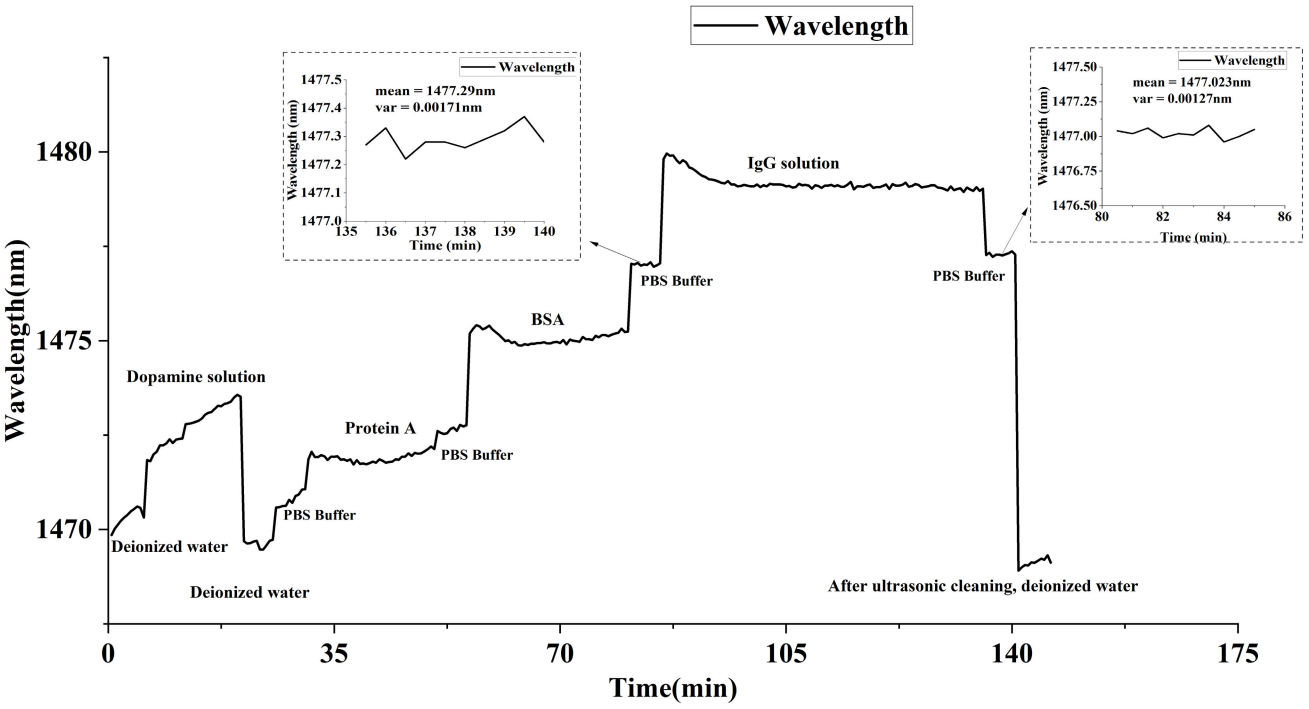

FIGURE 10. Spectral shift of the whole experiment.

fiber in PBS buffer is 1477.290 nm, and the corresponding variance is 0.04nm. This indicates that the wavelength shift caused by the immune response is 0.267 nm.

We have repeated the measuring process by the IgG solutions with different concentrations from 0.25 μg/ml to 2 μg/ml, which are shown in Fig. 11. It shows that the sensitivity of the sensor to IgG solution is -0.722 nm/(μg/ml).

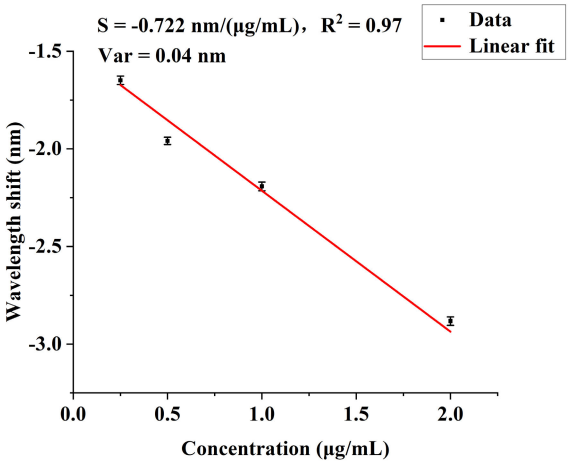

FIGURE 11. Peak wavelength shift with different concentrations of IgG.

The detection of biomolecules by the sensor can be evaluated based on the detection limit. LOD is defined as the minimum concentration of biomolecules that the sensor can detect. Taking into account the spectral resolution of the spectrometer, LOD is expressed as the ratio of the resolution of the spectrometer to the sensitivity of the sensor [29].

$$LOD = \frac{\Delta\lambda}{S} \tag{5}$$

where $\Delta\lambda$ is the wavelength resolution of the spectrometer and S is the sensitivity of the sensor. Because the minimum resolution of OSA is 0.02nm, the detection limit of the sensor is 28ng / ml, which realizes the detection of trace biomolecular solution.

After cleaning the optical fiber by the ultrasonic cleaner, we can see that the interference wavelength returns to the initial position in Fig. 10, which shows that our biosensor can be reused and has good stability.

D. SENSOR SPECIFICITY

In our experiment, cTnI antigen solution is employed to assess the specificity for the antibody-antigen combination process. The combination process cTnI antigen solution, as well as the IgG antigen solution, are shown in Fig.12. The optical fiber sensor is immersed in 0.125μg/mL cTnI antigen solution and 0.125μg/mL IgG antigen solution for 40 minutes respectively. Compared with the antigen solution, the interference wavelength shift of the cTnI antigen solution is much smaller. The interference wavelength of cTnI antigen solution fluctuates irregularly in a small range due to environmental

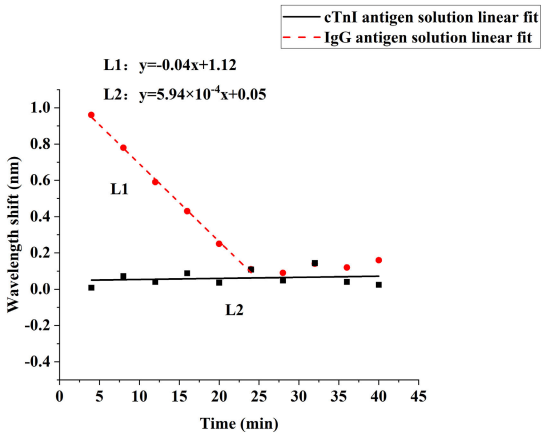

FIGURE 12. Temporal evolution of relative interference wavelength shift for the immobilized fiber sensor immersed in IgG antigen solution and cTnI antigen solution.

TABLE 1. Comparison of the LOD with different methods.

Method used	Analyte	LOD(μg/ml)	Ref
SPR	Human IgG	0.019	[30]
	Goat anti-Rabbit IgG	0.054	[31]
LSPR	Human IgG	0.12	[32]
	Human IgG	0.09	[33]
MZI	Human IgG	0.047	[34]
	Human IgG	0.028	This work

interference. This shows that the proposed fiber optic sensor has good specificity.

IV. CONCLUSION

We design and fabricate a fiber-optic biosensor with a low detection limit. The STF sensor has high refractive index sensitivity and is insensitive to temperature changes. The design, fabrication, and test of the biosensor are introduced in detail. The relationship between different structural parameters and the transmission spectrum of STF are studied. Using dopamine and protein to modify the STF sensor, and then the modified sensor is utilized to detect the human IgG antigen solutions with a detection limit of 28 ng/ml. Compared with other fiber-optic biosensors based on SPR, FBG, and MZI, the sensor is temperature-insensitive and has a compact size, low cost, high precision, fast response. By monitoring the shift of the selected wavelength, the real-time response of the antibody-antigen combination process can also be obtained in human IgG solutions with a low concentration of 0.25 μg/ml. The sensor has the advantages of simple structure, high mechanical strength, and good comprehensive performance. In addition, the proposed biosensor can also be used to detect other protein biomarkers by only changing the appropriate antibody on the fiber surface.

The detection limit is compared with other sensors reported for IgG immunosensing, shown in Table 1. It can be concluded from the table that the proposed sensor improves

the detection limit for IgG. This indicates that the proposed sensor is more advantageous in terms of trace detection of biomolecules and lower analyte concentration. The STF sensor has broad application prospects in medical diagnosis, immunoassay, and environmental monitoring.

REFERENCES

[1] N. L. Kazanskiy, S. N. Khonina, M. A. Butt, A. Kaźmierczak, and R. Piramidowicz, "State-of-the-art optical devices for biomedical sensing applications—A review," *Electronics*, vol. 10, no. 8, p. 973, 2021.
[2] Z. Guo, Y. Qin, P. Chen, J. Hu, Y. Zhou, X. Zhao, Z. Liu, Y. Fei, X. Jiang, and X. Wu, "Hyperboloid-drum microdisk laser biosensors for ultrasensitive detection of human IgG," *Small*, vol. 16, no. 26, 2020, Art. no. 2000239.
[3] C. R. Taitt, G. P. Anderson, and F. S. Ligler, "Evanescent wave fluorescence biosensors: Advances of the last decade," *Biosensors Bioelectron.*, vol. 76, pp. 103–112, Feb. 2016.
[4] S. Mohamed Nizar, B. Kesavaraman, E. Priyanka, and R. Jayasri, "Detection of immunoglobulin G (IgG) and immunoglobulin M (IgM) antibodies using circular photonic crystal fiber sensor," in *Proc. J. Phys., Conf.*, Jan. 2021, vol. 1717, Art. no. 012039.
[5] C. Li, M. Qian, Q. Hong, X. Xin, Z. Sun, Y. Li, B. Tang, and B. Gu, "Rapid, quantitative, and high-sensitivity detection of anti-phospholipase A2 receptor antibodies using a novel CdSe/ZnS-based fluorescence immunosorbent assay," *Sci. Rep.*, vol. 11, no. 1, p. 8778, Dec. 2021.
[6] R. R. Rasmi, V. B. Kadwad, J. Sarnaik, K. B. Shenoy, and H. M. Somashekarappa, "Development of radioimmunoassay for estimation of C-peptide in human serum," *J. Radioanal. Nucl. Chem.*, vol. 327, no. 2, pp. 923–928, Feb. 2021.
[7] J. Proch and P. Niedzielski, "Iron species determination by high performance liquid chromatography with plasma based optical emission detectors: HPLC–MIP OES and HPLC–ICP OES," *Talanta*, vol. 231, Aug. 2021, Art. no. 122403.
[8] H. Šípová-Jungová, L. Jurgová, K. Mrkvová, N. S. Lynn, B. Špačková, and J. Homola, "Biomolecular charges influence the response of surface plasmon resonance biosensors through electronic and ionic mechanisms," *Biosensors Bioelectron.*, vol. 126, pp. 365–372, Feb. 2019.
[9] Y. Zhao, H. Zhang, Y. Li, X. Yu, Y. Cai, X. Sha, S. Wang, Z. Zhan, J. Xu, and L. Liu, "AI powered electrochemical multi-component detection of insulin and glucose in serum," *Biosensors Bioelectron.*, vol. 186, Aug. 2021, Art. no. 113291.
[10] S. Jain, A. Paliwal, V. Gupta, and M. Tomar, "SPR studies on optical fiber coated with different plasmonic metals for fabrication of efficient biosensors," *Mater. Today: Proc.*, vol. 33, pp. 2180–2186, Jan. 2020.
[11] L. T. Nhiem and P. Sangkwon, "High performance detection of Alzheimer's disease biomarkers based on localized surface plasmon resonance," *J. Ind. Eng. Chem.*, vol. 91, pp. 182–190, Nov. 2020.
[12] R. Janeiro, R. Flores, and J. Viegas, "Silicon photonics waveguide array sensor for selective detection of VOCs at room temperature," *Sci. Rep.*, vol. 9, no. 1, p. 17099, Dec. 2019.
[13] J. Liao, Y. Xie, T. Huang, Z. Ding, M. Zeng, S. Wu, and X. Hu, "Highly sensitive near-infrared surface plasmon resonance (SPR) sensor based on birefringent six-core photonic crystal fibre," *J. Mod. Opt.*, vol. 67, no. 19, pp. 1463–1468, Nov. 2020.
[14] J. Ma, S. Wu, H. Cheng, X. Yang, S. Wang, and P. Lu, "Sensitivity-enhanced temperature sensor based on encapsulated S-taper fiber modal interferometer," *Opt. Laser Technol.*, vol. 139, Jul. 2021, Art. no. 106933.
[15] A. Tariq, J. Baydoun, C. Remy, R. Ghasemi, J. P. Lefevre, C. Mongin, A. Dauzères, and I. Leray, "Fluorescent molecular probe based optical fiber sensor dedicated to pH measurement of concrete," *Sens. Actuators B, Chem.*, vol. 327, Jan. 2021, Art. no. 128906.
[16] Y. Zhao, R.-J. Tong, M.-Q. Chen, and F. Xia, "Relative humidity sensor based on hollow core fiber filled with GQDs-PVA," *Sens. Actuators B, Chem.*, vol. 284, pp. 96–102, Apr. 2019.
[17] Z. Tong, P. Luan, Y. Cao, W. Zhang, and J. Su, "Dual-parameter optical fiber sensor based on concatenated down-taper and multimode fiber," *Opt. Commun.*, vol. 358, pp. 77–81, Jan. 2016.
[18] J. Li, M. Zhang, M. Wan, C. Lin, S. Huang, C. Liu, Q. He, X. Qiu, and X. Fang, "Ultrasensitive refractive index sensor based on enhanced Vernier effect through cascaded fiber core-offset pairs," *Opt Exp.*, vol. 28, no. 3, pp. 4145–4155, Feb. 2020.
[19] Y. Zheng, W. Xiao, and Z.-W. Zhu, "A simple macro-bending loss optical fiber crack sensor for the use over a large displacement range," *Opt. Fiber Technol.*, vol. 58, Sep. 2020, Art. no. 102280.
[20] M. Lobry, D. Lahem, M. Loyez, M. Debliquy, K. Chah, M. David, and C. Caucheteur, "Non-enzymatic D-glucose plasmonic optical fiber grating biosensor," *Biosensors Bioelectron.*, vol. 142, Oct. 2019, Art. no. 111506.
[21] W. Yu, T. Lang, J. Bian, and W. Kong, "Label-free fiber optic biosensor based on thin-core modal interferometer," *Sens. Actuators B, Chem.*, vol. 228, pp. 322–329, Jun. 2016.
[22] H. Suzuki, M. Sugimoto, Y. Matsui, and J. Kondoh, "Effects of gold film thickness on spectrum profile and sensitivity of a multimode-optical-fiber SPR sensor," *Sens. Actuators B, Chem.*, vol. 132, no. 1, pp. 26–33, May 2008.
[23] R. Yang, Y.-S. Yu, Y. Xue, C. Chen, Q.-D. Chen, and H.-B. Sun, "Single S-tapered fiber Mach–Zehnder interferometers," *Opt. Lett.*, vol. 36, no. 23, pp. 4482–4484, 2011.
[24] X. Liu, Y. Liu, and Z. Wang, "A biosensor based on a modified S-taper fiber for target protein detection," *Nanotechnol. Precis. Eng.*, vol. 3, no. 3, pp. 162–166, Sep. 2020.
[25] J. Li, W. Zhang, S. Gao, Z. Bai, L. Wang, H. Liang, and T. Yan, "Simultaneous force and temperature measurement using S fiber taper in fiber Bragg grating," *IEEE Photon. Technol. Lett.*, vol. 26, no. 3, pp. 309–312, Feb. 1, 2014.
[26] K. Tian, M. Zhang, G. Farrell, R. Wang, E. Lewis, and P. Wang, "Highly sensitive strain sensor based on composite interference established within S-tapered multimode fiber structure," *Opt. Exp.*, vol. 26, no. 26, pp. 33982–33992, Dec. 2018.
[27] Y. Li, Y. Miao, F. Wang, J. Wang, Z. Ma, L. Wang, X. Di, and K. Zhang, "Serial-tilted-tapered fiber with high sensitivity for low refractive index range," *Opt. Exp.*, vol. 26, no. 26, pp. 34776–34788, Dec. 2018.
[28] H. Luo, X. Li, W. Zou, X. Li, Z. Hong, and J. Chen, "Temperature-insensitive microdisplacement sensor based on locally bent microfiber taper modal interferometer," *IEEE Photon. J.*, vol. 4, no. 3, pp. 772–778, Jun. 2012.
[29] A. M. Shrivastav, S. P. Usha, and B. D. Gupta, "Highly sensitive and selective erythromycin nanosensor employing fiber optic SPR/ERY imprinted nanostructure: Application in milk and honey," *Biosensors Bioelectron.*, vol. 90, pp. 516–524, Apr. 2017.
[30] H. Song, Q. Wang, and W.-M. Zhao, "A novel SPR sensor sensitivity-enhancing method for immunoassay by inserting MoS_2 nanosheets between metal film and fiber," *Opt. Lasers Eng.*, vol. 132, Sep. 2020, Art. no. 106135.
[31] K. Liu, J. Zhang, J. Jiang, T. Xu, S. Wang, P. Chang, Z. Zhang, J. Ma, and T. Liu, "Multi-layer optical fiber surface plasmon resonance biosensor based on a sandwich structure of polydopamine-$MoSe_2$@Au nanoparticles-polydopamine," *Biomed. Opt. Exp.*, vol. 11, no. 12, pp. 6840–6851, 2020.
[32] M. Lu, H. Zhu, L. Hong, J. Zhao, J.-F. Masson, and W. Peng, "Wavelength-tunable optical fiber localized surface plasmon resonance biosensor via a diblock copolymer-templated nanorod monolayer," *ACS Appl. Mater. Interfaces*, vol. 12, no. 45, pp. 50929–50940, Nov. 2020.
[33] M. Lu, H. Zhu, M. Lin, F. Wang, L. Hong, J.-F. Masson, and W. Peng, "Comparative study of block copolymer-templated localized surface plasmon resonance optical fiber biosensors: CTAB or citrate-stabilized gold nanorods," *Sens. Actuators B, Chem.*, vol. 329, Feb. 2021, Art. no. 129094.
[34] B.-T. Wang and Q. Wang, "An interferometric optical fiber biosensor with high sensitivity for IgG/anti-IgG immunosensing," *Opt. Commun.*, vol. 426, pp. 388–394, Nov. 2018.

HAOWEI LIU received the bachelor's degree from Jiangsu University, in 2019. He is currently pursuing the master's degree with Harbin Institute of Technology, Shenzhen, China. His main research interest includes biosensor of tapered micro-nano fiber.

YUNXU SUN (Senior Member, IEEE) received the bachelor's degree from Beijing University of Technology, in 1995, and the Ph.D. degree from Tsinghua University, in 2006. He is currently an Associate Professor with Harbin Institute of Technology, Shenzhen, China. His research interests include non-linear optics, special fiber design and fiber sensing, quantum optics, and silicon photonics.

JUN GUO received the master's degree in mechanical and electronic engineering from Harbin Institute of Technology, China, in 2018. She is currently an Engineer with Tsinghua Shenzhen International Graduate School, Shenzhen, China. Her research interest includes optical metrology.

WEI LIU received the bachelor's and Ph.D. degrees from Harbin Institute of Technology, in 2010 and 2015, respectively. He is currently an Assistant Professor with the Harbin Institute of Technology, Shenzhen, China. His research interests include computational optical imaging, multimodal optical imaging, optical genetic technology, and medical imaging equipment development.

LE LIU received the Ph.D. degree from the Department of Physics, Tsinghua University, Beijing, China, in 2010. He is currently an Associate Professor with the Tsinghua Shenzhen International Graduate School, Shenzhen, China. His current research interests include optical sensing principle and methodology, and their applications in the energy materials and bio-sensing.

YAN MENG received the master's degree from Harbin Institute of Technology, Shenzhen, China, in 2021. Her main research interest includes micro structure tapered fiber sensor based on inter mode interference.

XIN YU received the bachelor's degree from Nanjing Agricultural University, in 2019. She is currently pursuing the master's degree with Harbin Institute of Technology, Shenzhen, China. Her main research interest includes speckle demodulation of micro-nano fiber sensor.